Wang Cong (Orcid ID: 0000-0002-1193-6862)
Beringer Jason (Orcid ID: 0000-0002-4619-8361)
Hutley Lindsay, B. (Orcid ID: 0000-0001-5533-9886)
Cleverly James (Orcid ID: 0000-0002-2731-7150)
Li Jing (Orcid ID: 0000-0001-9736-5732)
Liu Qinhuo (Orcid ID: 0000-0002-3713-9511)
Sun Ying (Orcid ID: 0000-0002-9819-1241)

Phenology Dynamics of Dryland Ecosystems Along North Australian Tropical Transect Revealed by Satellite Solar-Induced Chlorophyll Fluorescence

Cong Wang[1,2,3], Jason Beringer[4], Lindsay B. Hutley[5], James Cleverly[6], Jing Li[2], Qinhuo Liu[2,3,7], and Ying Sun[1,*]

[1]School of Integrative Plant Science, Soil and Crop Sciences Section, Cornell University, Ithaca, NY.
[2]State Key Laboratory of Remote Sensing Science, Institute of Remote Sensing and Digital Earth, Chinese Academy of Sciences, Beijing, China.
[3]College of Resources and Environment, University of Chinese Academy of Sciences (UCAS), Beijing, China.
[4]School of Agriculture and Environment, University of Western Australia, Crawley, Western Australia, Australia.
[5]School of Environment, Charles Darwin University, Darwin, Northern Territory, Australia.
[6]Terrestrial Ecosystem Research Network, School of Life Sciences, University of Technology, Sydney, Australia.
[7]Joint Center for Global Change Studies (JCGCS), Beijing, China.

[*]Corresponding author: Ying Sun (ys776@cornell.edu)

Key Points

- Satellite SIF matches seasonal phenology of eddy covariance GPP better than EVI and NIRv along a rainfall gradient in northern Australia.
- Increasing soil exposure in inland xeric shrublands deteriorates the capability of satellite EVI and NIRv for phenology characterization.
- High resolution satellite SIF is needed to accurately depict phenology in heterogeneous landscapes with complex vegetation–soil mosaic.

This article has been accepted for publication and undergone full peer review but has not been through the copyediting, typesetting, pagination and proofreading process which may lead to differences between this version and the Version of Record. Please cite this article as doi: 10.1029/2019GL082716

Abstract

Accurate phenological characterization of dryland ecosystems has remained a challenge due to the complex composition of plant functional types, each having distinct phenological dynamics, sensitivity to climate and disturbance. Solar-induced chlorophyll fluorescence (SIF), a proxy for photosynthesis, offers potential to alleviate such challenge. We here explore this potential using dryland systems along the North Australian Tropical Transect (NATT) with SIF derived from Orbiting Carbon Observatory-2. SIF identified the seasonal onset and senescence of Gross Primary Production at eddy covariance sites with improved accuracy over Enhanced Vegetation Index (EVI) and Near Infrared Reflectance of terrestrial Vegetation (NIRv) from Moderate Resolution Imaging Spectroradiometer, especially at inland xeric shrublands. At regional scale, SIF depicted both earlier onset and senescence across NATT. We hypothesized that SIF outperformed EVI and NIRv mainly because, unlike reflectance, it is not contaminated by background soil and its total signal is contributed by mixed plant species in additive way.

Plain Language Summary

Australian dryland ecosystems are critical in regulating the global land carbon sink dynamics. However, it is challenging to accurately characterize their phenology from spaceborne measurements. On the one hand, tropical savannas and semi-arid ecosystems (e.g., grasslands, shurblands) are typically comprised of a complex mixture of species (woody trees and C_4 grasses) with each having distinct morphologies and physiological responses to climate condition; on the other hand, such ecosystems are highly sensitive to irregular rainfall events, and are often subject to disturbances such as fires and storms. In this study, we utilized the North Australian Tropical Transect (NATT) rainfall gradient as a 'natural laboratory' to assess the ability of satellite solar-induced chlorophyll fluorescence (SIF) to capture the phenological dynamics of dryland vegetation, in comparison with traditional reflectance-based vegetation indices, i.e. Enhanced Vegetation Index (EVI) and Near Infrared Reflectance of terrestrial Vegetation (NIRv). Results showed that satellite SIF outperformed EVI and NIRv for characterizing seasonal onset and senescence along NATT and therefore had potential for improving large-scale mapping of phenology dynamics of dryland ecosystems over traditional remote sensing of reflectance based vegetation indices.

1 Introduction

Australian dryland ecosystems play an important role in regulating the trend and interannual variability of the global land carbon sink (Ahlström et al., 2015; Poulter et al., 2014), mainly due to their strong sensitivity of ecosystem productivity (or Gross Primary Production, GPP) to variation in climate and disturbance (Beringer et al., 2016; Chen et al., 2016; Ma et al., 2013). Accurate characterization of the phenology of dryland ecosystems, i.e., the start and end dates of a growing season, and the associated growing season length, is critical for assessing the dynamics of carbon exchanges in these ecosystems. In Australia, environmental drivers including both regular (e.g. rainfall, fire) and irregular (e.g. storms and cyclones) events can alter ecosystem composition, structure, and functions (Moore et al., 2016). These features lead to high spatial heterogeneity of dryland vegetation productivity and a complex response to disturbance regimes and climate variability.

Satellite remote sensing of Solar-Induced chlorophyll Fluorescence (SIF) offers potential to unravel these complex ecosystem dynamics (Frankenberg et al., 2011). SIF is a signal emitted by green plants when solar photons are absorbed by chlorophylls within photosynthetic machinery, thus providing a mechanistic proxy for photosynthesis (Porcar-Castell et al., 2014). Satellite SIF retrievals have been demonstrated to be highly correlated with GPP at large scale and could be used to reveal GPP dynamics in response to environmental variations (e.g., Frankenberg et al., 2011; Guanter et al., 2012; Sun et al., 2015). Specific to dryland systems, studies have quantified the relationship between satellite SIF and GPP (e.g., Sanders et al., 2016; Smith et al., 2018; Verma et al., 2017; Li et al., 2018). For example, Verma et al. (2017) found a robust linear correlation between NASA's Orbiting Carbon Observatory-2 (OCO-2) SIF and GPP derived from an eddy covariance (EC) flux tower at a semi-arid grassland site in Australia over a season. Sanders et al. (2016) examined the SIF-GPP relationship of a number of EC towers in Australia using SIF records

from the Global Ozone Monitoring Experiment-2 (GOME-2) onboard MetOp-A. They also found a linear SIF-GPP relationship but reported that managed biomes typically had higher correlations than natural vegetation. Smith et al. (2018) reported that for dryland systems in the southwest US, GOME-2 SIF tended to better capture the seasonal and interannual variations in GPP than the traditional Enhanced Vegetation Index (EVI).

Although these studies demonstrated the correlation between SIF and GPP in space and time, the application of satellite SIF for elucidating the rapid phenological transitions of dryland vegetation has not yet been explored. The unique strength of SIF in depicting phenological transitions over conventional vegetation indices (VIs) has previously been reported for a diverse number of biomes (Joiner et al., 2014), primarily focusing on evergreen conifers, temperate forests and crops (Jeong et al., 2017; Lu et al., 2018; Urban et al., 2018; Walther et al., 2016; Joiner et al., 2014). In contrast, phenology characterization for dryland ecosystems using SIF has not been conducted. The comparatively low productivity and thus lower SIF signal of dryland vegetation may suffer from relatively high noise level when using existing satellite SIF products (Sun et al., 2018). Moreover, the growth and phenology of dryland ecosystems are highly sensitive to irregular rainfall events (Brown et al., 2010; Eamus et al., 2013; Rogers & Beringer, 2017), in contrast to evergreen coniferous and temperate forests which are primarily driven by temperature variations. Consequently, an examination is needed to evaluate whether the relatively weaker and noisier SIF signal in dryland ecosystems can still accurately detect phenology.

In this study, we defined dryland ecosystems in Australia as a structural continuum with varying mixtures of trees, grasses and shrubs, including woodland savannas, shrublands, and grasslands, following Ma et al. (2013). We aim to: 1) assess the ability of satellite SIF in capturing phenological dynamics of dryland systems; 2) determine the utility of SIF to advance phenological characterization in dryland ecosystems compared to the numerous

current approaches that used reflectance-based VIs (e.g., Archibald & Scholes, 2007; Ferreira et al., 2013; Huete et al., 2002; Ma et al., 2013). To achieve this, we utilized the North Australian Tropical Transect (NATT) as a testbed, which provides a natural laboratory with wide range of vegetation structure, function, and phenological variability (Mott et al., 1985; Williams et al., 1997; Hutley et al., 2011). We compared SIF-based phenological metrics with those derived from EVI, which have previously been employed to characterize the phenology of Australian drylands (Ma et al., 2013; Broich et al., 2015). We also compared SIF with the recently developed Near Infrared Reflectance of terrestrial Vegetation index (NIRv), i.e. the product of total scene NIR reflectance and NDVI (Normalized Difference Vegetation Index), which was reported to be more closely coupled to GPP than NDVI alone, especially for sparsely vegetated areas (Badgley et al., 2017). This study did not include NDVI because it has already been demonstrated to be far more sensitive to soil background than EVI and NIRv (e.g., Huete et al., 2002; Badgley et al., 2017) and performed poorly in heterogeneous systems (Hmimina et al., 2013). We conducted our investigation first at EC towers along NATT and then scaled up the findings to the regional scale.

2 Datasets and Methods

2.1 Site characteristics and measurements at selected OzFlux EC towers along NATT

We selected six well-characterized EC tower sites from the OzFlux network (Gorsel et al., 2018) along NATT: Howard Springs (AU-How), Litchfield (AU-Lit), Daly River (AU-Dap), Dry River (AU-Dry), Stuart Plains (AU-Stp) and Alice Springs (AU-ASM) (Fig. S1 and Table S1) (Beringer et al. 2011a, b; Cleverly et al. 2013; Hutley et al., 2011). These sites cover a transect from coastal humid savannas to inland arid/semi-arid grasslands and shrublands (Fig. S1a), with an increasing coverage of bare soil (Fig. S1b).

At each site, we obtained half-hourly EC GPP between 2014 and 2018 from OzFlux. GPP fluxes were derived from the Dynamic Integrated Gap-filling and partitioning for OzFlux（DINGO) based on the Level 3 data（Beringer et al., 2017). We aggregated half-hourly GPP to a 16-day composite to match the temporal resolution of the SIF products from OCO-2 (details in Section 2.2.1). In addition, we used soil moisture (i.e., volumetric water content, m^3/m^3) measured at each EC site to examine the degree to which soil moisture impacted the temporal variation of vegetation activities. Here we used the top 10cm soil moisture, because the depths of measurements vary from site to site and only the top layer (10cm) is consistently available for all EC sites.

2.2 Description of satellite datasets

2.2.1 OCO-2 SIF products

We utilized both the native OCO-2 SIF (Sun et al., 2018) and spatially contiguous SIF products ($\overline{SIF}_{OCO2\_005}$) at 0.05° and 16-day resolution gap-filled from OCO-2 by Yu et al. (2018), available since September 2014. OCO-2 SIF was retrieved at both 757 and 771 nm by using solar Fraunhofer lines. This study used the average of the two wavelengths, with the 771nm SIF scaled to 757nm by a factor of 1.5 to reduce noise, following Sun et al. (2018). Here we extracted the native OCO-2 SIF pixels that 1) are within a 0.5° radius centered at each EC site, 2) are in nadir mode, and 3) have the same land cover type (details in section 2.2.2) as the EC tower. A relatively wide radius is required here to ensure sufficient number of retrievals for effectively reducing retrieval noise, although it will inevitably introduce scale mismatch between satellite and ground measurements. SIF values corresponding to each site were computed as the average of all extracted pixels. The instantaneous OCO-2 SIF was converted to daily averages using a daily correction factor (Sun et al., 2018).

This study primarily relied on $\overline{SIF}_{OCO2\_005}$, a global spatially contiguous daily-average SIF product, for phenological characterization, because the existing native SIF retrievals have either spatial gaps (thus leading to lack of overlap with EC towers, e.g., OCO-2) or low spatial resolution (thus challenging to be applied to examine the highly dynamic dryland systems that are commonly spatially heterogeneous, e.g., GOME-2). $\overline{SIF}_{OCO2\_005}$ is generated by a machine learning method constrained by physiological understandings, and could accurately preserve the spatiotemporal variability of the original OCO-2 SIF across the globe (Yu, et al., 2019). $\overline{SIF}_{OCO2\_005}$ has been validated with independent airborne measurements from Chlorophyll Fluorescence Imaging Spectrometer (CFIS). The spatial contiguity of $\overline{SIF}_{OCO2\_005}$ makes it possible to examine the phenological synchrony of satellite SIF with in-situ GPP, in contrast to the native OCO-2 SIF that are only available along orbits, which precludes the use of EC towers that are not directly underpassing OCO-2. Indeed, only AU-Stp (Verma et al., 2017), among the six selected sites along NATT, was in direct underpass of OCO-2 orbits. Also, lower data availability of the native OCO-2 SIF product prevented time series fitting for deriving phenological metrics (details in 2.4). For each EC site, we averaged all $\overline{SIF}_{OCO2\_005}$ pixels if 1) they have the same land cover type as the EC tower, and 2) they are within a 3x3 window centered at the EC tower. In addition, $\overline{SIF}_{OCO2\_005}$ was also used for spatial mapping of phenological metrics at the regional scale, which is not possible with the native OCO-2 SIF retrievals due to substantial orbital gaps.

2.2.2 MODIS EVI, NIRv, and Land Cover Type

Both EVI and NIRv in this study were computed from the Moderate Resolution Imaging Spectroradiometer (MODIS) Terra Vegetation Indices (MOD13C1, V006) at 0.05° and 16-day resolution. We used the 9th day of each 16-day composite period for each timestamp for subsequent phenology calculations. For each EC site, we averaged all pixels if 1) they have

the same land cover type as the EC tower, 2) they are within a 3x3 window centered at the EC tower, and 3) they are in high quality according to the Quality Assurance (QA) flag. The land cover type was determined from the MCD12C1 V005 product at 0.05° resolution.

2.2.3 Soil fractional coverage

In order to assess the impact of background bare soil on phenological characterization, we used soil fractional coverage product developed by the Commonwealth Scientific and Industrial Research Organisation (CSIRO). This dataset is derived from the MODIS Nadir BRDF-Adjusted Reflectance with a linear unmixing methodology (Guerschman et al. 2015). This product is provided monthly at 0.25 °. Here we calculated the annual mean fraction of bare soil from monthly datasets in 2015.

2.4 Phenological metrics

We employed the Singular Spectrum Analysis (SSA) (Elsner & Tsonis, 1996) to smooth the time series and to derive the phenological metrics. SSA essentially uses the Singular Value Decomposition (SVD) approach to reconstruct the time series from an originally noisy dataset. This approach selects the leading SVD components that contain most of the information of the trend and periodicity of the time series. The SSA approach is particularly suitable here for Australian dryland systems where satellite measurements are usually noisy (especially SIF) or interspersed with missing values due to cloud or aerosol contamination (such as EVI and NIRv). Ma et al. (2013) have successfully employed SSA to derive phenological metrics using EVI in northern Australia. This study adopted this approach and applied it to EC GPP, $\overline{\mathrm{SIF}}_{\mathrm{OCO2\_005}}$, and MODIS NIRv and EVI. Here we set the window length as 24 consistently for all variables to capture the periodicity of phenology and reduce most of the random noise. We selected the first three leading components to reconstruct the

time series. Three key phenological metrics were extracted for each variable: the start of growing season (SOS), defined as the date halfway between the minimum value and the fastest greening rate; the end of growing season (EOS), the date halfway between the fastest brown-down rate and minimum value; the length of growing season (LOS), the difference between EOS and SOS.

3 Results and Discussions

3.1 Seasonal variation and phenological metrics extracted from SIF, EVI, NIRv and GPP at EC sites

The six EC sites showed distinct seasonality of GPP along NATT (Fig. 1), with declining seasonal amplitude of GPP from the northern mesic savanna to the xeric shrublands, consistent with previous studies (Beringer et al., 2016; Ma et al., 2013). $\overline{SIF}_{OCO2\_005}$ exhibited a stronger temporal consistency with EC GPP than EVI or NIRv did at most EC sites, evidenced by a greater R^2 of GPP with SIF than with EVI or NIRv from 2014 to 2018 (Fig. 1). In particular, $\overline{SIF}_{OCO2\_005}$ substantially outperformed EVI and NIRv at the xeric shrubland site AU-ASM, where the former captured more than 50% of the variability in GPP fluxes while the latter could only explain less than 20% (Fig. 1f). However, the correlation between SIF and GPP appeared to degrade for AU-Dry (Fig. 1d). This site is located near the center of orbital gaps where no native OCO-2 measurements were acquired (Fig. 1d). Therefore $\overline{SIF}_{OCO2\_005}$ at this site might be more susceptible to uncertainties associated with gap-filling because of the long distance of the EC tower from orbits. Interestingly, both MODIS EVI and NIRv were very similar both intra- and interannually, and exhibited similar R^2 with EC GPP although NIRv was designed to better characterize GPP dynamics for sparse vegetation (Badgley et al., 2017) such as dryland systems. We further found that $\overline{SIF}_{OCO2\_005}$ tended to

exhibit stronger consistency (i.e., greater R^2) with soil moisture than EC GPP, EVI or NIRv did at most EC sites from 2014 to 2018 (Table S2).

We further evaluated the phenological metrics derived from $\overline{SIF}_{OCO2\_005}$, EVI, and NIRv by comparing their deviation from GPP-derived phenology for each EC site (Table 1). Such deviation was evaluated using the mean absolute error (MAE) across years. In general, there was considerable year-to-year and site-to-site variability of phenology depicted by satellite measurements, agreeing with Ma et al. (2013). At the northernmost mesic sites (i.e., AU-How and AU-Lit), SOS was similar among SIF, EVI and NIRv, indicating their similar capability for monitoring the timing of seasonal green-up. Similar patterns were found for EOS at AU-How and AU-Das. The largest discrepancies of both SOS and EOS were observed at AU-Stp and AU-ASM (Table 1), where EVI and NIRv exhibited a substantial delay relative to GPP. In particular, at AU-ASM, EVI-based metrics can have up to 84 days delay in SOS (40 days delay in EOS) relative to EC GPP, a magnitude comparable to Ma et al. (2013). In contrast, SIF appeared to have a closer correspondence with GPP at this site, with MAE less than 20 days for SOS and EOS compared to GPP. One possible reason is that the large soil coverage would have contaminated the reflectance-based VIs such as EVI and NIRv at this site. Indeed, AU-Asm, among all sites, has the largest soil fraction (Fig. S1b). However, SIF contains zero contribution from non-fluorescing targets, as discussed in detail in section 3.2. These findings are consistent with the higher R^2 between SIF and GPP in Fig. 1. An exception occurred at AU-Dry where EVI and NIRv outperformed SIF in identifying the SOS and EOS of GPP, again probably because of potential uncertainties present in $\overline{SIF}_{OCO2\_005}$ originated from gap-filling, as explained above.

3.2 Spatial patterns of vegetation phenology across the NATT at the regional scale

To scale up our findings from individual EC sites, we utilized $\overline{SIF}_{OCO2\_005}$, EVI and NIRv to derive regional maps of SOS and EOS across the NATT (Fig. 2). We observed a delaying pattern in both SOS and EOS from the mesic north to the xeric south for all variables (Fig. S2), consistent with the latitudinal shift reported by Ma et al. (2013). As expected, there was a striking consistency between EVI and NIRv in SOS, EOS, and LOS (Fig. S2).

Interestingly, we found substantial differences between SIF and EVI (similarly NIRv) in the derived phenological metrics (Fig. 2), which might be a consequence of the susceptibility of EVI and NIRv to high heterogeneity in the mixture of soil type/texture and vegetation species (among other factors such as fires) that may confound the spectral signature of optical reflectance. To test this possibility, we computed the differences of SOS (and EOS) between EVI and $\overline{SIF}_{OCO2\_005}$, denoted as ΔSOS (ΔEOS), and found that increasing soil exposure could result in larger ΔSOS and ΔEOS. Such dependence was statistically significant for ΔEOS (R^2=0.82, $p<0.01$, Fig. 3b), which could explain the increasing delay of EVI EOS relative to SIF towards the inland xeric shrublands in Fig. 2b. This examination is useful to interpret the advantage of SIF for characterizing phenology of dryland systems. For reflectance, there is differential contribution of mixed plant species as well as soil to the total observed signal (Smith et al., 1990). However, SIF does not suffer from these issues, since a) non-fluorescing targets (such as soil) do not contribute to the observed SIF signal, and b) different plant species contribute to the total SIF in additive way, which is not the case for optical reflectance (Frankenberg et al., 2014). The aggregated reflectance-based VIs from mixed species and soil does not necessarily linearly translate to aggregated GPP in the same footprint unless fractional coverages of each land component are equal. Another plausible reason is that the reflectance-based VIs may only capture

morphological development but not physiological development of plant canopies. Therefore, any time lag between morphological and physiological development could lead to a bias in phenological estimation (Joiner et al., 2014), which is particularly crucial for dryland systems that typically comprise a complex mixture of species which have distinct morphological traits and physiological responses to climate conditions. This may contribute to the insignificant relationship between ΔSOS and soil fraction in Fig. 3a.

3.3 Outlook for future work

Future work is needed to further improve the accuracy of tracking the phenological transitions with SIF. Achieving this will require higher spatial and temporal resolution SIF with less noise. Yu et al. (2019) reported that $\overline{\mathrm{SIF}}_{\mathrm{OCO2\_005}}$ tended to under-predict high values and over-predict low values of SIF although the mean value was well predicted for shrubland. This may have resulted from the lower magnitude of SIF and thus higher impact of SIF retrieval noise in shrublands. In addition, the relatively coarse temporal resolution (16-days) could mask rapid changes in both SIF and VIs driven by high rainfall variability and may also influence SSA fitting, whose robustness will benefit from higher frequency datasets. SIF retrievals from TROPOspheric Monitoring Instrument (TROPOMI) (Köhler et al., 2018), which has a daily revisit cycle, may significantly improve the phenological characterization, although this study did not directly employ TROPOMI SIF as its mission period is too short (data available since March 2018) to conduct similar phenology analysis. This study did not attempt to separate trees and grasses to obtain their individual phenology dynamics because SIF itself as well as GPP is an integrated measure contributed by all vegetation components, with distinct morphology and function mixed within a pixel. Furthermore, the kilometer-scale resolution of SIF is not sufficient to accurately decouple the highly heterogeneous

composition of woody and herbaceous species, a challenge similarly faced by MODIS VIs (Ma et al., 2013). On the other hand, the unique features of SIF as an integrated proxy for GPP greatly simplify the needs to explicitly separate trees and grasses.

4 Conclusions

This study demonstrated that satellite SIF is capable of improving large-scale mapping and characterization of phenology dynamics of dryland ecosystems over traditional remote sensing of VIs, including EVI and NIRv. The main advantage of SIF lies in that, in contrast to reflectance-based VIs, it does not suffer from contamination of background soil, and its total signal is contributed by different plant species in additive way. This greatly alleviates the challenges for depicting phenology dynamics of dryland vegetation which is highly heterogeneous with complex vegetation–soil mosaic. Albeit using the NATT as a testbed, this study should have global implications and could be extended to other dryland ecosystems. Future applications of satellite SIF in phenological studies will further benefit from the next generation of sensor deployment from missions with higher spatial and/or temporal resolutions such as TROPOMI with growing records or the upcoming FLuorescence EXplorer (FLEX).

Acknowledgments

C. Wang is supported by UCAS Joint PhD Training Program, National Key Research and Development Program (2018YFA0605503), GF6 Project under Grant 30-Y20A03-9003-17/18; Y. Sun is supported by the NASA MEaSURE program. The OzFlux network is supported by the Australian Government through the Terrestrial Ecosystem Research Network (TERN) and the National Collaborative Research Infrastructure Strategy (NCRIS). Data sources: Ozflux GPP comes from http://data.ozflux.org.au/portal/home.jspx, $\overline{SIF}_{OCO2\_005}$ is available at https://cornell.app.box.com/s/cavtg50y80udbdirg022gm5whugmth02, the

native OCO-2 SIF is available at https://co2.jpl.nasa.gov, all MODIS products come from https://e4ftl01.cr.usgs.gov/MOTA/ and the Fractional Cover dataset is from http://qld.auscover.org.au/public/data/modis/fractional_cover/global/.

References

Ahlström, A., Raupach, M. R., Schurgers, G., Smith, B., Arneth, A., Jung, M., et al. (2015). The dominant role of semi-arid ecosystems in the trend and variability of the land CO2 sink. Science, 348(6237), 895-899.

Archibald, S., & Scholes, R. (2007). Leaf green‐up in a semi‐arid African savanna‐separating tree and grass responses to environmental cues. Journal of Vegetation Science, 18(4), 583-594.

Badgley, G., Field, C. B., & Berry, J. A. (2017). Canopy near-infrared reflectance and terrestrial photosynthesis. Science advances, 3(3), e1602244.

Baker, N. R. J. A. R. P. B. (2008). Chlorophyll fluorescence: a probe of photosynthesis in vivo. 59, 89-113.

Beringer, J., Hacker, J., Hutley, L. B., Leuning, R., Arndt, S. K., Amiri, R., et al. (2011). SPECIAL—Savanna

Beringer, J., Hutley, L. B., Hacker, J. M., & Neininger, B. (2011). Patterns and processes of carbon, water and energy cycles across northern Australian landscapes: From point to region. Agricultural and Forest Meteorology, 151(11), 1409-1416.

Beringer, J., Hacker, J., Hutley, L. B., Leuning, R., Arndt, S. K., Amiri, R., et al. (2011). SPECIAL—Savanna patterns of energy and carbon integrated across the landscape. Bulletin of the American Meteorological Society, 92(11), 1467-1485.

Beringer, J., Hutley, L. B., McHugh, I., Arndt, S. K., Campbell, D., Cleugh, H. A., et al. (2016). An introduction to the Australian and New Zealand flux tower network–OzFlux. Biogeosciences.

Beringer, J., McHugh, I., Hutley, L. B., Isaac, P., & Kljun, N. (2017). Dynamic INtegrated Gap-filling and partitioning for OzFlux (DINGO). Biogeosciences, 14(6), 1457-1460.

Broich, M., Huete, A., Paget, M., Ma, X., Tulbure, M., Coupe, N. R., et al. (2015). A spatially explicit land surface phenology data product for science, monitoring and natural resources management applications. Environmental Modelling & Software, 64, 191-204.

Brown, M. E., de Beurs, K., & Vrieling, A. (2010). The response of African land surface phenology to large scale climate oscillations. Remote sensing of Environment, 114(10), 2286-2296.

Chen, C., Cleverly, J., Zhang, L., Yu, Q., & Eamus, D. (2016). Modelling seasonal and inter-annual variations in carbon and water fluxes in an Arid-Zone Acacia Savanna Woodland, 1981–2012. Ecosystems, 19(4), 625-644.

Cleverly, J., Boulain, N., Villalobos‐Vega, R., Grant, N., Faux, R., Wood, C., et al. (2013). Dynamics of component carbon fluxes in a semi‐arid Acacia woodland, central Australia. Journal of Geophysical Research: Biogeosciences, 118(3), 1168-1185.

Eamus, D., Cleverly, J., Boulain, N., Grant, N., Faux, R., & Villalobos-Vega, R. (2013). Carbon and water fluxes in an arid-zone Acacia savanna woodland: An analyses of seasonal patterns and responses to rainfall events. Agricultural and Forest Meteorology, 182, 225-238.

Elsner, J. B., & Tsonis, A. A. (1996). Phase Space Reconstruction. In Singular Spectrum Analysis (pp. 143-155): Springer.

Ferreira, M. E., Ferreira Jr, L. G., Miziara, F., & Soares-Filho, B. S. (2013). Modeling landscape dynamics in the central Brazilian savanna biome: future scenarios and perspectives for conservation. Journal of Land Use Science, 8(4), 403-421.

Frankenberg, C., Fisher, J. B., Worden, J., Badgley, G., Saatchi, S. S., Lee, J. E., et al. (2011). New global observations of the terrestrial carbon cycle from GOSAT: Patterns of plant fluorescence with gross primary productivity. Geophysical Research Letters, 38(17).

Frankenberg, C., O'Dell, C., Berry, J., Guanter, L., Joiner, J., Köhler, P., et al. (2014). Prospects for chlorophyll fluorescence remote sensing from the Orbiting Carbon Observatory-2. Remote sensing of Environment, 147, 1-12.

Gorsel, E. v., Cleverly, J., Beringer, J., Cleugh, H., Eamus, D., Hutley, L. B., et al. (2018). Preface: OzFlux: a network for the study of ecosystem carbon and water dynamics across Australia and New Zealand. Biogeosciences, 15(1), 349-352.

Guanter, L., Frankenberg, C., Dudhia, A., Lewis, P. E., Gómez-Dans, J., Kuze, A., et al. (2012). Retrieval and global assessment of terrestrial chlorophyll fluorescence from GOSAT space measurements. Remote sensing of Environment, 121, 236-251.

Guerschman, J. P., Hill, M. J., Renzullo, L. J., Barrett, D. J., Marks, A. S., & Botha, E. J. J. R. S. o. E. (2009). Estimating fractional cover of photosynthetic vegetation, non-photosynthetic vegetation and bare soil in the Australian tropical savanna region upscaling the EO-1 Hyperion and MODIS sensors. 113(5), 928-945.

Guerschman, J. P., Scarth, P. F., McVicar, T. R., Renzullo, L. J., Malthus, T. J., Stewart, J. B., et al. (2015). Assessing the effects of site heterogeneity and soil properties when unmixing photosynthetic vegetation, non-photosynthetic vegetation and bare soil fractions from Landsat and MODIS data. Remote Sensing of Environment, 161, 12-26.

Hmimina, G., Dufrêne, E., Pontailler, J.-Y., Delpierre, N., Aubinet, M., Caquet, B., et al. (2013). Evaluation of the potential of MODIS satellite data to predict vegetation phenology in different biomes: An investigation using ground-based NDVI measurements. Remote sensing of Environment, 132, 145-158.

Huete, A., Didan, K., Miura, T., Rodriguez, E. P., Gao, X., & Ferreira, L. G. (2002). Overview of the radiometric and biophysical performance of the MODIS vegetation indices. Remote sensing of Environment, 83(1-2), 195-213.

Hutley, L. B., Beringer, J., Isaac, P. R., Hacker, J. M., & Cernusak, L. A. (2011). A sub-continental scale living laboratory: Spatial patterns of savanna vegetation over a rainfall gradient in northern Australia. Agricultural and Forest Meteorology, 151(11), 1417-1428.

Jeong, S.-J., Schimel, D., Frankenberg, C., Drewry, D. T., Fisher, J. B., Verma, M., et al. (2017). Application of satellite solar-induced chlorophyll fluorescence to understanding large-scale variations in vegetation phenology and function over northern high latitude forests. Remote sensing of Environment, 190, 178-187.

Joiner, J., Guanter, L., Lindstrot, R., Voigt, M., Vasilkov, A., Middleton, E., et al. (2013). Global monitoring of terrestrial chlorophyll fluorescence from moderate-spectral-resolution near-infrared satellite measurements: methodology, simulations, and application to GOME-2. Atmospheric Measurement Techniques, 6(10), 2803-2823.

Joiner, J., Yoshida, Y., Vasilkov, A., Schaefer, K., Jung, M., Guanter, L., et al. (2014). The seasonal cycle of satellite chlorophyll fluorescence observations and its relationship to vegetation phenology and ecosystem atmosphere carbon exchange. Remote sensing of Environment, 152, 375-391.

Köhler, P., Frankenberg, C., Magney, T. S., Guanter, L., Joiner, J., & Landgraf, J. J. G. R. L. (2018). Global Retrievals of Solar‐Induced Chlorophyll Fluorescence With TROPOMI: First Results and Intersensor Comparison to OCO‐2. 45(19), 10,456-410,463.

Krause, G., & Weis, E. J. A. r. o. p. b. (1991). Chlorophyll fluorescence and photosynthesis: the basics. 42(1), 313-349.

Li, X., Xiao, J., & He, B. (2018). Chlorophyll fluorescence observed by OCO-2 is strongly related to gross primary productivity estimated from flux towers in temperate forests. Remote sensing of Environment, 204, 659-671.

Li, X., Xiao, J., He, B., Altaf Arain, M., Beringer, J., Desai, A. R., et al. (2018). Solar‐induced chlorophyll fluorescence is strongly correlated with terrestrial photosynthesis for a wide variety of biomes: First global analysis based on OCO‐2 and flux tower observations. Global change biology.

Lu, X., Liu, Z., Zhou, Y., Liu, Y., An, S., & Tang, J. (2018). Comparison of Phenology Estimated from Reflectance-Based Indices and Solar-Induced Chlorophyll Fluorescence (SIF) Observations in a Temperate Forest Using GPP-Based Phenology as the Standard. Remote Sensing, 10(6), 932.

Ma, X., Huete, A., Yu, Q., Coupe, N. R., Davies, K., Broich, M., et al. (2013). Spatial patterns and temporal dynamics in savanna vegetation phenology across the North Australian Tropical Transect. Remote sensing of Environment, 139, 97-115.

Moore, C. E., Brown, T., Keenan, T. F., Duursma, R. A., Dijk, A. I. v., Beringer, J., et al. (2016). Reviews and syntheses: Australian vegetation phenology: new insights from satellite remote sensing and digital repeat photography. Biogeosciences, 13, 5085-5102.

Mott, J., Williams, J., Andrew, M., & Gillison, A. (1985). Australian savanna ecosystems. Ecology and management of the world's savannas'.(Eds JC Tothill and JJ Mott.) pp, 56-82.

Paget, M. J., & King, E. A. (2008). MODIS Land data sets for the Australian region.

Porcar-Castell, A., Tyystjärvi, E., Atherton, J., Van der Tol, C., Flexas, J., Pfündel, E. E., et al. (2014). Linking chlorophyll a fluorescence to photosynthesis for remote sensing applications: mechanisms and challenges. 65(15), 4065-4095.

Poulter, B., Frank, D., Ciais, P., Myneni, R. B., Andela, N., Bi, J., et al. (2014). Contribution of semi-arid ecosystems to interannual variability of the global carbon cycle. Nature, 509(7502), 600.

Rogers, C. D. W., & Beringer, J. (2017). Describing rainfall in northern Australia using multiple climate indices. Biogeosciences, 14(3), 597-615.

Sanders, A. F., Verstraeten, W. W., Kooreman, M. L., Van Leth, T. C., Beringer, J., & Joiner, J. (2016). Spaceborne sun-induced vegetation fluorescence time series from 2007 to 2015 evaluated with australian flux tower measurements. Remote Sensing, 8(11), 895.

Schaaf, C., & Wang, Z. (2015). MCD43A4 MODIS/Terra+ Aqua BRDF/Albedo Nadir BRDF Adjusted RefDaily L3 Global 500 m V006. NASA EOSDIS Land Processes DAAC.

Smith, M. O., Ustin, S. L., Adams, J. B., & Gillespie, A. R. (1990). Vegetation in deserts. I. A regional measure of abundance from multispectral images. Remote sensing of Environment, 31(1), 1-26.

Smith, W., Biederman, J., Scott, R., Moore, D., He, M., Kimball, J., et al. (2018). Chlorophyll fluorescence better captures seasonal and interannual gross primary productivity dynamics across dryland ecosystems of southwestern North America. Geophysical Research Letters, 45(2), 748-757.

Sun, Y., Frankenberg, C., Wood, J. D., Schimel, D. S., Jung, M., Guanter, L., et al. (2017). OCO-2 advances photosynthesis observation from space via solar-induced chlorophyll fluorescence. Science, 358(6360), eaam5747.

Sun, Y., Frankenberg, C., Jung, M., Joiner, J., Guanter, L., Köhler, P., & Magney, T. (2018). Overview of Solar-Induced chlorophyll Fluorescence (SIF) from the Orbiting Carbon Observatory-2: Retrieval, cross-mission comparison, and global monitoring for GPP. Remote sensing of Environment, 209, 808-823.

Tan, B., Morisette, J. T., Wolfe, R. E., Gao, F., Ederer, G. A., Nightingale, J., & Pedelty, J. A. (2011). An enhanced TIMESAT algorithm for estimating vegetation phenology metrics from MODIS data. IEEE Journal of Selected Topics in Applied Earth Observations and Remote Sensing, 4(2), 361-371.

Urban, D., Guan, K., & Jain, M. (2018). Estimating sowing dates from satellite data over the US Midwest: A comparison of multiple sensors and metrics. Remote sensing of Environment, 211, 400-412.

Verma, M., Schimel, D., Evans, B., Frankenberg, C., Beringer, J., Drewry, D. T., et al. (2017). Effect of environmental conditions on the relationship between solar‐induced fluorescence and gross primary productivity at an OzFlux grassland site. Journal of Geophysical Research: Biogeosciences, 122(3), 716-733.

Walther, S., Voigt, M., Thum, T., Gonsamo, A., Zhang, Y., Köhler, P., et al. (2016). Satellite chlorophyll fluorescence measurements reveal large‐scale decoupling of photosynthesis and greenness dynamics in boreal evergreen forests. Global change biology, 22(9), 2979-2996.

Whitley, R. J., MACINNIS‐NG, C. M., Hutley, L. B., Beringer, J., Zeppel, M., Williams, M., et al. (2011). Is productivity of mesic savannas light limited or water limited? Results of a simulation study. Global change biology, 17(10), 3130-3149.

Williams, R., Myers, B., Muller, W., Duff, G., & Eamus, D. (1997). Leaf phenology of woody species in a north Australian tropical savanna. Ecology, 78(8), 2542-2558.

Yu, L., Wen, J., Chang, C. Y., Frankenberg, C., & Sun, Y. (2019). High-Resolution Global Contiguous SIF of OCO-2. Geophysical Research Letters, 46(3), 1449-1458.

Table 1. Summary of differences (in days) of SOS and EOS derived from $\overline{SIF}_{OCO2\_005}$, NIRv, EVI, relative to that derived from GPP. Negative values indicate that the variable of interest has an earlier onset (for SOS) or offset (for EOS) than that of GPP, and vice versa. Values in bold highlight the smallest deviation from GPP-based phenological metrics among $\overline{SIF}_{OCO2\_005}$, EVI, and NIRv. The mean absolute error (MAE) across years summarizes the overall discrepancy of SOS and EOS between each variable and GPP. Note that the missing SOS and EOS values for AU-Dry, AU-Stp, and AU-ASM in later years were primarily caused by incomplete time series that prevented successful SSA fitting.

Site	Data	SOS				EOS				
		2015~2016	2016~2017	2017~2018	MAE	2014~2015	2015~2016	2016~2017	2017~2018	MAE
AU-How	SIF-GPP	-8	**2**	**-6**	**5.33**	-36	-20	-8	**9**	18.25
	NIRv-GPP	**7**	-10	**-6**	7.67	-20	-10	**1**	25	14.00
	EVI-GPP	12	-9	**-6**	9.00	**-12**	**-2**	**1**	31	**11.50**
AU-Lit	SIF-GPP	-16	**-1**	-9	8.67		-17	-23	-7	15.67
	NIRv-GPP	**-9**	-2	**-5**	**5.33**		**0**	**-7**	-5	**4.00**
	EVI-GPP	**-9**	6	-11	8.67		7	**-7**	**0**	4.67
AU-Das	SIF-GPP	-7	**0**	**-3**	**3.33**	-39	**0**	**-6**	8	**13.25**
	NIRv-GPP	**-2**	31	4	12.33	-22	17	12	9	15.00
	EVI-GPP	-1	33	6	13.33	**-14**	17	16	**9**	14.00
AU-Dry	SIF-GPP	-37	-37	-38	37.33	-53	-16	-15		28.00
	NIRv-GPP	**0**	5	-5	3.33	-22	5	-10		12.33
	EVI-GPP	1	**2**	**2**	**1.67**	**-20**	**4**	**-5**		**9.67**
AU-Stp	SIF-GPP	**-5**	-24	**-10**	**13.00**	-9	**-7**	**-8**		**8.00**
	NIRv-GPP	22	**15**	29	22.00	**8**	10	10		9.33
	EVI-GPP	30	**15**	28	24.33	26	11	10		15.67
AU-ASM	SIF-GPP	**11**	**26**		**18.50**	**-1**	**30**			**15.50**
	NIRv-GPP	56	33		44.50	38	34			36.00
	EVI-GPP	84	40		62.00	39	40			39.50

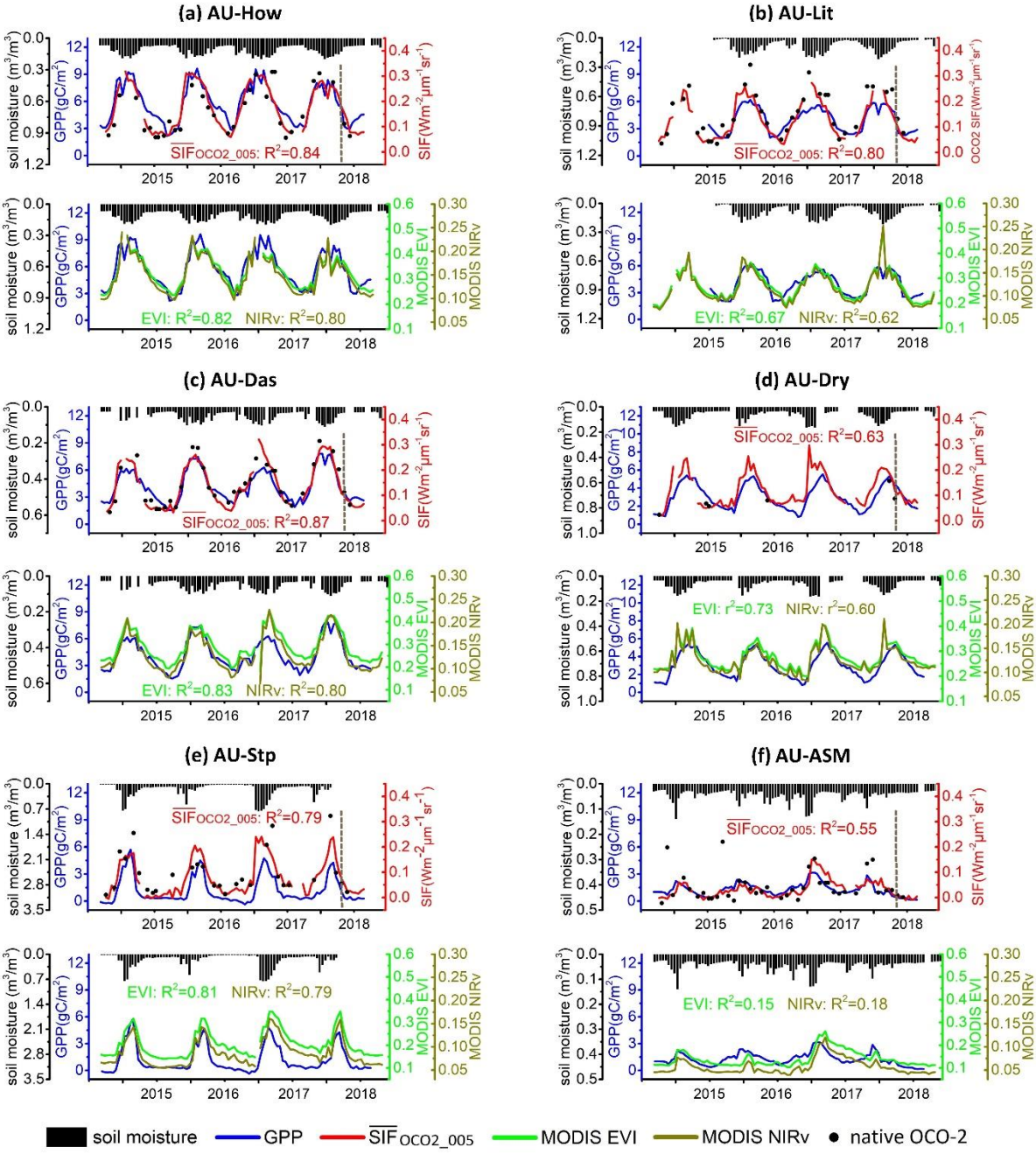

Figure 1. Time series of 16-day aggregated values at selected Ozflux EC towers along NATT. R^2 refers to the coefficients of determination from linear regressions between EC GPP and remote sensing variables. The dotted line highlights the month when TROPOMI SIF retrievals became available. Note there are very few native OCO-2 SIF retrievals covering AU-Dry.

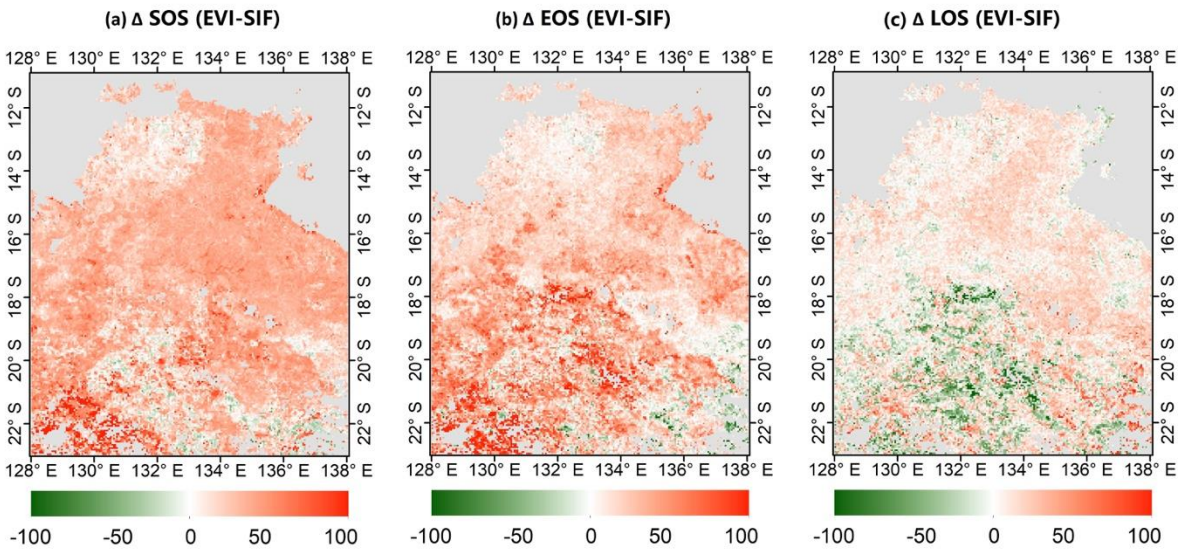

Figure 2. Spatial patterns of the differences of mean phenological metrics between EVI and $\overline{SIF}_{OCO2\_005}$ (days) from 2015 to 2017, denoted as (a) ΔSOS, (b) ΔEOS, (c) ΔLOS.

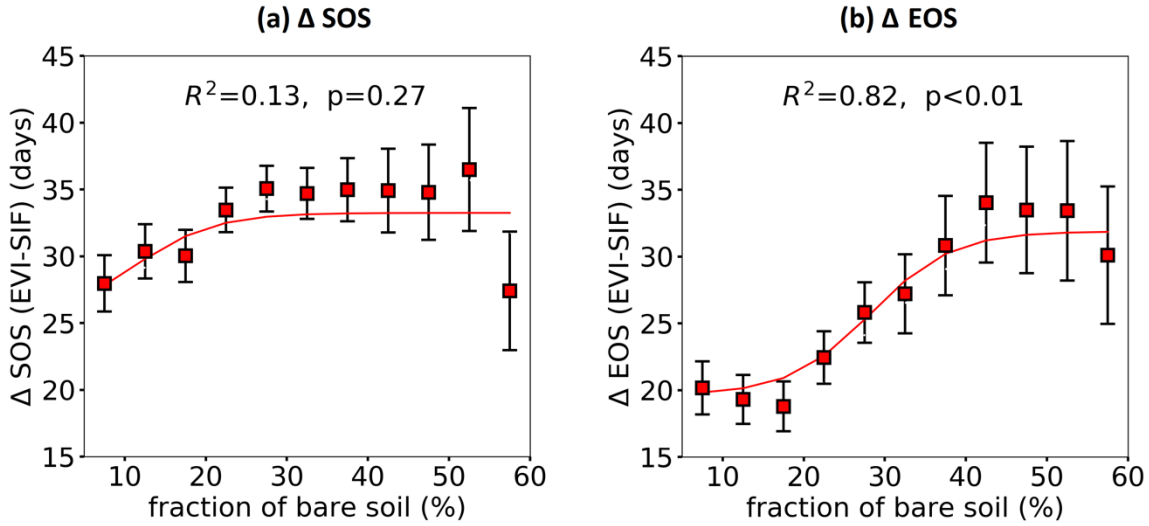

Figure 3. The relationship of (a) ΔSOS and (b) ΔEOS between EVI and $\overline{SIF}_{OCO2\_005}$ with bare soil fraction. Datasets in Figure 2 were binned into bare soil fraction categories. The red squares and error bars represent the mean and standard error of each bin. The red line shows the nonlinear fit for the mean of each bin using logistic functions.